Directed flow at midrapidity in event-by-event hydrodynamics

Fernando G. Gardim,[1] Frédérique Grassi,[1] Yogiro Hama,[1] Matthew Luzum,[2] and Jean-Yves Ollitrault[3]
[1]*Instituto de Física, Universidade de São Paulo, C.P. 66318, 05315-970, São Paulo-SP, Brazil*
[2]*CEA, IPhT, Institut de physique theorique de Saclay, F-91191 Gif-sur-Yvette, France*
[3]*CNRS, URA2306, IPhT, Institut de physique theorique de Saclay, F-91191 Gif-sur-Yvette, France*
(Received 24 March 2011; published 15 June 2011)

Fluctuations in the initial geometry of a nucleus-nucleus collision have been recently shown to result in a new type of directed flow (v_1) that, unlike the usual directed flow, is also present at midrapidity. We compute this new v_1 versus transverse momentum and centrality for Au-Au collisions at RHIC using the hydrodynamic code NeXSPheRIO. We find that the event plane of v_1 is correlated with the angle of the initial dipole of the distribution, as predicted, though with a large dispersion. It is uncorrelated with the reaction plane. Our results are in excellent agreement with results inferred from STAR correlation data.

DOI: 10.1103/PhysRevC.83.064901 PACS number(s): 25.75.Ld, 24.10.Nz, 24.10.Jv

I. INTRODUCTION

Analyses of correlations between particles emitted in ultrarelativistic heavy-ion collisions at large relative rapidity reveal azimuthal structure that can be interpreted as solely due to collective flow [1]. Event-by-event hydrodynamics [2–6] is a natural framework for studying collective flow. In each event, particles are emitted independently according to some momentum distribution determined by a fluid freeze-out surface. The most general azimuthal distribution can be written as a Fourier series with respect to the azimuthal angle ϕ of the particle momentum:

$$2\pi \frac{dP}{d\phi} = 1 + 2\sum_{n=1}^{+\infty} v_n \cos[n(\phi - \Psi_n)], \tag{1}$$

where v_n is the magnitude of anisotropic flow [7] and Ψ_n is the reference angle in harmonic n. An equivalent definition is

$$v_n e^{in\Psi_n} = \langle e^{in\phi} \rangle, \tag{2}$$

where angular brackets denote an average with the probability law $dP/d\phi$. Once a convention is chosen for the sign of v_n, these equations define Ψ_n up to $2\pi/n$. Both v_n and Ψ_n may depend on the transverse momentum p_t and the rapidity y.

Typically the largest term in the series (1) is elliptic flow, v_2 [8], and Ψ_2 is usually referred to as the event plane. The only other harmonics measured so far at RHIC are v_1 and v_4 [9]. However, it has recently been pointed out that fluctuations in the initial density profile generally result in different reference angles Ψ_n for every n. In particular, one expects additional triangular (v_3) [10] and dipole (v_1) [11] components from fluctuations, both uncorrelated with the event plane Ψ_2. Although triangular flow has already been studied in a hydrodynamic framework [5,12,13], there has not yet been a prediction for this new v_1 that arises from fluctuations.

The variation of directed flow with rapidity can be uniquely separated into even and odd parts:

$$v_1(y)e^{i\Psi_1(y)} = v_1^{\text{even}}(y)e^{i\Psi_1^{\text{even}}(y)} + v_1^{\text{odd}}(y)e^{i\Psi_1^{\text{odd}}(y)}, \tag{3}$$

where $v_1^{\text{even}}(y)$, $\Psi_1^{\text{even}}(y)$, and $\Psi_1^{\text{odd}}(y)$ are even functions of y, while $v_1^{\text{odd}}(-y) = -v_1^{\text{odd}}(y)$. Usual directed flow [9,14–16] is $v_1^{\text{odd}}(y)$, and the corresponding Ψ_1^{odd} is correlated with the reaction plane and Ψ_2. Teaney and Yan recently argued [11] that fluctuations in the initial geometry create an even part $v_1^{\text{even}}(y)$, which depends weakly on y. This even part does not contribute to existing directed flow measurements but can be isolated experimentally [17] using an event-plane method where the weights are independent of rapidity (assuming that the detector is symmetric in rapidity). Here $\Psi_1^{\text{even}}(y)$ is predicted to have little correlation with the reaction plane or Ψ_2, unlike $\Psi_1^{\text{odd}}(y)$. It is also expected to have little dependence on p_t or y.

There is no dedicated analysis of $v_1^{\text{even}}(y)$ yet, but indirect evidence has been obtained [17] from recent STAR correlation data [18], and both the magnitude and p_t dependence of v_1 are in qualitative agreement with theoretical expectations [11].

We present the first quantitative predictions for v_1^{even} in Au-Au collisions at the top RHIC energy, using the hydrodynamic code NeXSPheRIO [2]. Calculations of v_1^{odd} will be presented separately [19]. NeXSPheRIO solves the equations of relativistic ideal hydrodynamics using initial conditions provided by the event generator NeXus [20]. Fluctuations in initial conditions are studied by generating many NeXus events and solving the equations of ideal hydrodynamics independently for each event. NeXSPheRIO provides a good description of rapidity and transverse momentum spectra [21] and elliptic flow v_2 [22]. In addition, it reproduces the ridge observed in two-particle correlations [23], which is produced by initial fluctuations, followed by collective flow. Teaney and Yan's dipole asymmetry is created by fluctuations followed by collective flow, much in the same way as the ridge [10], and should therefore be present in NeXSPheRIO.

NeXSPheRIO does not include effects of shear viscosity, which was recently implemented in event-by-event hydrodynamics [5]. While shear viscosity produces a sizable reduction of elliptic flow [24,25], we expect its effect to be smaller on v_1, following the general observation that damping is larger for higher harmonics [13].

In Sec. II, we explain how $v_1^{\rm even}$ is calculated. In Sec. III, we present predictions for its p_t dependence and centrality dependence in Au-Au collisions at the top RHIC energy and compare with existing STAR data. In Sec. IV, we study the correlation of directed flow with the initial dipole asymmetry defined by Teaney and Yan [11]. Our conclusions are presented in Sec. V. We use v_1, Ψ_1 as a shorthand notation for $v_1^{\rm even}$, $\Psi_1^{\rm even}$ throughout this paper.

II. MEASURING v_1 IN EVENT-BY-EVENT HYDRODYNAMICS

The code NeXSPheRIO emits particles at the end of the hydrodynamical evolution using a Monte Carlo generator, and one can analyze events much in the same way as in an actual experiment. Particles are emitted independently. The only nonflow correlation in NeXSPheRIO is the correlation induced by resonance decays [26]. In principle, $v_1(p_t, y)$ and $\Psi_1(p_t, y)$ can be computed directly from Eq. (2) by averaging over particles emitted from the Monte Carlo generator. The only practical limitation is computer time, which results in finite statistical errors. In order to obtain reliable results, we integrate v_1 over the pseudorapidity interval $-1 < \eta < 1$, corresponding approximately to the acceptance of the time projection chamber of the STAR experiment [27]. We estimate Ψ_1 by computing a weighted average $\Psi_{\rm EP,1}$ inspired by the event-plane method used in experimental analyses [28]:

$$Q\cos\Psi_{\rm EP,1} \equiv \sum_{|\eta|<1} w_j \cos\phi_j,$$
$$Q\sin\Psi_{\rm EP,1} \equiv \sum_{|\eta|<1} w_j \sin\phi_j, \qquad (4)$$

where the sum is over particles emitted in the pseudorapidity interval $-1 < \eta < 1$, ϕ_j are the azimuthal angles of outgoing particles, $Q \geqslant 0$, and w_j is a weight [17] depending on the particle transverse momentum p_t:

$$w(p_t) = p_t - \frac{\langle p_t^2\rangle}{\langle p_t\rangle}, \qquad (5)$$

where angular brackets denote an average over particles of all events in the centrality window and in the same pseudorapidity interval $-1 < \eta < 1$. This particular choice of the weight eliminates both $v_1^{\rm odd}$ in Eq. (3), and nonflow correlations from momentum conservation (though the latter are not implemented in this calculation). We compute $\langle p_t^2\rangle$ and $\langle p_t\rangle$ by averaging over all events in the 0%–40% centrality window, where p_t spectra depend little on centrality [29]. Here $w(p_t)$ changes sign at $p_t = \langle p_t^2\rangle/\langle p_t\rangle \simeq 0.85$ GeV/c.

In order to achieve small statistical errors, we run the Monte Carlo generator many times for each event. In practice, the summation in Eq. (4) runs over 7×10^5 particles. This ensures almost perfect reconstruction of Ψ_1 for most events. We then measure

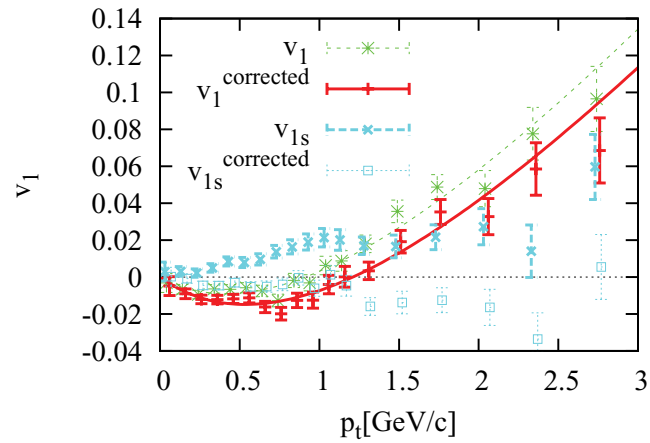

FIG. 1. (Color online) Hadron $v_1(p_t)$ and $v_{1s}(p_t)$ in $|\eta| < 1$ for a single NeXSPheRIO event with impact parameter $b = 1$ fm. Results are shown with and without correcting for the net transverse momentum (see text). Vertical bars are statistical errors.

$$v_1(p_t) \equiv \langle\cos(\phi - \Psi_{\rm EP,1})\rangle, \quad v_{1s}(p_t) \equiv \langle\sin(\phi - \Psi_{\rm EP,1})\rangle, \qquad (6)$$

where brackets denote an average over particles in a p_t bin. If Ψ_1 in Eq. (2) is independent of p_t, then it coincides with $\Psi_{EP,1}$, and $v_{1s}(p_t)$ vanishes identically.

Figure 1 displays $v_1(p_t)$ and $v_{1s}(p_t)$ for the first event we analyzed. Here $v_1(p_t)$ has roughly the expected behavior: It vanishes linearly at low p_t [30], changes sign around 1 GeV [11], and increases linearly at high p_t [31]. The solid line is a three-parameter rational fit with the same properties:

$$v_1(p_t) = \frac{a p_t (p_t - b)}{p_t + c}. \qquad (7)$$

Here $v_{1s}(p_t)$ is not compatible with 0: It is in fact positive for all p_t, which means that there is a small nonzero net transverse momentum in the direction perpendicular to $\Psi_{EP,1}$. Averages in Eq. (6) are taken over the pseudorapidity interval $-1 < \eta < 1$.

This net transverse momentum could come from several sources. In principle, net transverse momentum can be generated by the initial dynamics, if a corresponding transverse momentum is transferred to "spectator" nucleons. An additional net transverse momentum can be generated in the pseudorapidity interval used here if, during the evolution of the system, net momentum is transferred to particles that end up outside this range of pseudorapidity. In addition, however, there can be spurious momentum generated in NeXSPheRIO during the thermalization stage, as an unphysical side affect of the transition from the microscopic model NeXuS to hydrodynamics. A detailed explanation and the alternative procedure that exactly conserves conservation of energy and momentum is presented in the Appendix, though its implementation and a thorough investigation of energy and momentum nonconservation in the standard scheme are left for future work.

We are not aware of any measurement of the net transverse momentum of charged hadrons in a symmetric pseudorapidity interval. In particular, there is no experimental evidence that it

is larger than statistical fluctuations. Since our v_1 results can be significantly modified by a net momentum, which is yet unknown experimentally, it is useful to present another set of results with a different (smaller) value of the net momentum.

A simple way to correct for the net transverse momentum is by boosting the system in the transverse direction, and by adjusting the boost velocity so that the net momentum vanishes in the new frame. This is difficult in practice, however, because the "system" here is the set of particles in the pseudorapidity interval $-1 < \eta < 1$, and η is not invariant under a transverse boost. We adopt the following approximate procedure: We define the boost velocity by $\vec{v} \equiv \sum_{|\eta|<1} \vec{p} / \sum_{|\eta|<1} E$. We then boost all the particles, select particles with $|\eta| < 1$ in the new frame, and compute v_1 for these particles. Since this set of particles differs from the original set, the net transverse momentum is not strictly zero in the new frame, but it should be significantly smaller. Results after correction are shown in Fig. 1. Here $v_{1s}(p_t)$ is smaller in absolute magnitude, but still nonzero, because the correction is approximate.

The next step is to average over events. This is done in the same way as would be done in an experiment. The scalar-product method [32] provides a simple prescription for doing the average, and it is known to give the same results as the event-plane method if the event-plane resolution is not too large [33]. Equation (7) of Ref. [32] gives

$$v_1\{EP\} = \frac{\langle v_1 Q \rangle}{\sqrt{\langle Q^2 \rangle}}, \tag{8}$$

where angular brackets denote average over particles in the numerator and over events in the denominator. Due to the (almost perfect) event-plane resolution, there is no need to use subevents: The flow vector of one subevent is approximately half of the total flow vector, $Q_a \simeq Q_b \simeq Q/2$.

Results presented in this paper are obtained from a set of 120 different NeXSPheRIO events, each corresponding to a different initial geometry. Each event is an Au-Au collision at 200 GeV per nucleon in the 0%–60% centrality range. Events are uniformly distributed in centrality, and centrality is determined according to the number of participant nucleons. Compared with an actual experiment, we work with a limited number of events, but we generate a very large multiplicity in every event, so that our determination of v_1 is not limited by statistical fluctuations. In practice, 75% of the events that we use have a resolution parameter [30] $\chi \equiv Q/\sqrt{\sum (w_j)^2}$ larger than 3, implying an event plane resolution $\langle \cos \Delta\phi \rangle$ larger than 0.97. Since χ scales like Q, events with the lowest resolution have a negligible contribution to $v_1\{EP\}$.

III. PREDICTIONS FOR v_1 AT RHIC

Our results for $v_1(p_t)$ and $v_{1s}(p_t)$ in the centrality bin 0%–40% are presented in Fig. 2, with and without correcting for the net transverse momentum in each event. After averaging over events, $v_{1s}(p_t)$ is much smaller in absolute magnitude than $v_1(p_t)$. In fact, $v_{1s}(p_t)$ should be identically zero by parity symmetry. Any difference can be attributed to statistical uncertainty due to the finite number of events. Results in this centrality range are very similar with or without correction for the net transverse momentum. The p_t dependence of v_1 is in qualitative agreement with theoretical expectations [11]: It is linear and negative at low p_t, reaches a minimum between -0.01 and -0.02, then increases and crosses 0 at $p_t \simeq 1.1$ GeV/c.

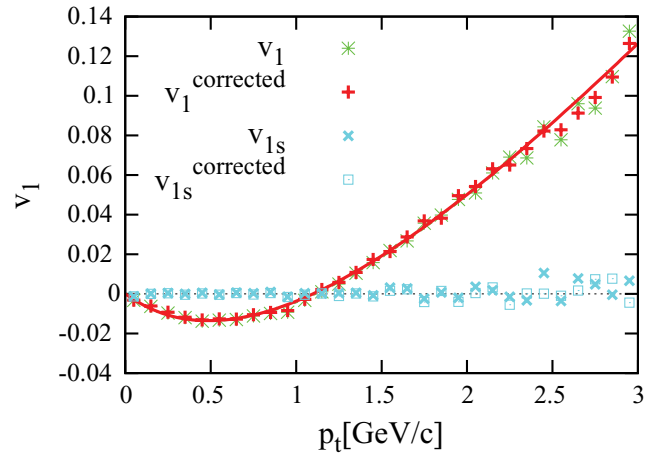

FIG. 2. (Color online) $v_1(p_t)$ and $v_{1s}(p_t)$ of hadrons in $|\eta| < 1$ averaged over events in the 0%–40% centrality window. As in Fig. 1, results are shown with and without correcting for the net transverse momentum. Solid lines are fits using Eq. (7).

Figure 3 compares our hydro calculation for the centrality range 20%–60% to values of v_1 [17] inferred from STAR correlation data in the same centrality range [18]. As in Fig. 2, results are shown with and without correcting for the net transverse momentum in each event. For this centrality range, $v_1(p_t)$ is slightly larger when the correction is made, resulting in excellent agreement with data in the range $0 < p_t < 2$ GeV/c.

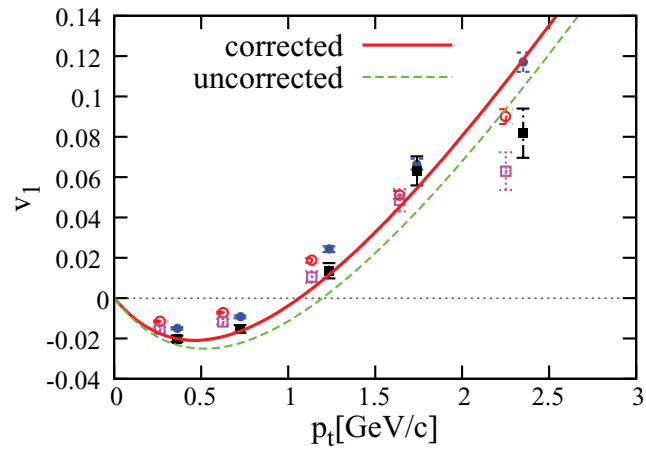

FIG. 3. (Color online) $v_1(p_t)$ of hadrons in $|\eta| < 1$ in Au-Au collisions (20%–60% centrality) inferred from STAR correlation data [18]. Different sets of points correspond to different trigger particles and different assumptions concerning the v_1 of trigger particles (see Ref. [17]). Solid curve: Our hydro calculation averaged over events in the same centrality window, corrected for net transverse momentum (see text) and fitted using Eq. (7). The dashed curve represents the uncorrected value.

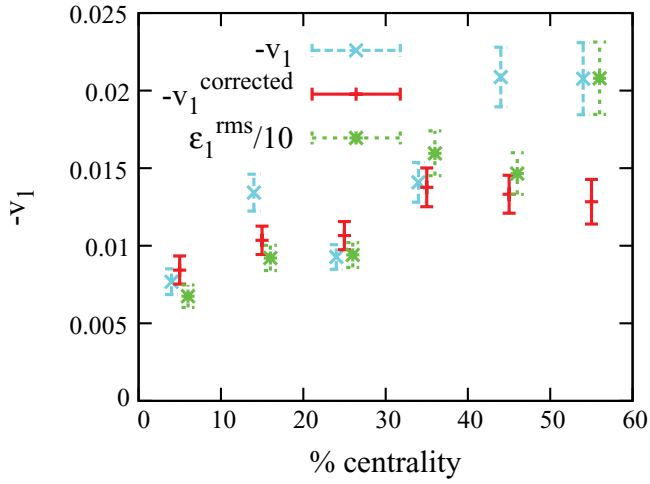

FIG. 4. (Color online) $|v_1| = -v_1$ of hadrons with $0 < p_t < 1$, $|\eta| < 1$ versus centrality. Dashed lines: raw NeXSPheRIO results. Solid lines: After correcting for net transverse momentum (see text). Dotted lines: RMS dipole asymmetry (scaled down by a factor 10) vs centrality. Error bars on v_1 are obtained by assuming that the relative statistical errors on v_1 and $\varepsilon_1^{\rm rms}$ are identical.

Figure 4 displays the centrality dependence of $-v_1$, averaged over hadrons with $p_t < 1$ GeV/c, $|\eta| < 1$. Results are smoother when NeXSPheRIO results are corrected for the net transverse momentum. Here $-v_1$ increases mildly with centrality. The reason is that v_1 is created by fluctuations, which are larger for more peripheral collisions. The centrality dependence of v_1 is comparable to that of v_3 [13].

IV. CORRELATION WITH THE INITIAL DIPOLE ASYMMETRY

Teaney and Yan [11] have shown that fluctuations in the initial geometry of a nucleus-nucleus collision are expected to create this new type of directed flow. Fluctuations break the symmetry of the initial density profile, and as a result there is, in general, one direction where the profile is steepest. This effect can be quantified as a dipole asymmetry in the initial density [11]:

$$\varepsilon_1 e^{i\Phi_1} = -\frac{\langle r^3 e^{i\phi}\rangle}{\langle r^3\rangle}, \tag{9}$$

where the averages in the right-hand side are taken over the initial transverse energy density profile, and (r, ϕ) is a polar coordinate system around the center of the distribution, defined by $\langle r e^{i\phi}\rangle = 0$. If one chooses ε_1 to be positive, then Φ_1 generally corresponds to the steepest direction for a smooth profile, and ε_1 is the magnitude of the dipole asymmetry. In general, ε_1 differs from 0—even at midrapidity—due to fluctuations.

For smooth initial conditions, one expects $\Psi_1 = \Phi_1$ in each event. One also expects $v_1 \propto \varepsilon_1$, in the same way as elliptic flow is proportional to the participant eccentricity [34]. Experimentally, v_1 will be extracted from a two-particle correlation, which scales like $(v_1)^2$, so that the experimentally

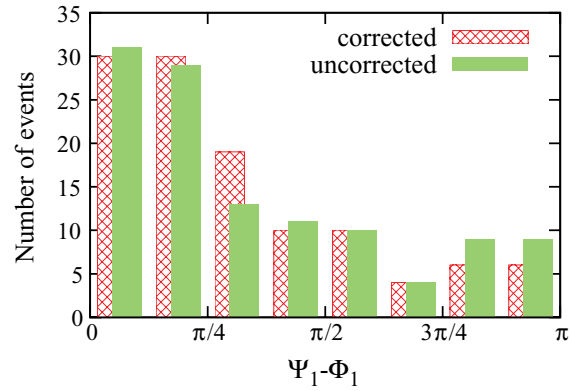

FIG. 5. (Color online) Distribution of the relative angle between the event plane Ψ_1 and the initial dipole Φ_1 for the centrality range 0%–60%. As in previous figures, results are shown before and after correcting for net transverse momentum.

measured v_1 should scale like the rms dipole asymmetry $\varepsilon_1^{\rm rms} \equiv \sqrt{\langle(\varepsilon_1)^2\rangle}$ [35]. Figure 4 displays the rms dipole asymmetry versus centrality. The values are similar to those obtained using a Monte Carlo Glauber calculation [11]. In particular, $\varepsilon_1^{\rm rms}$ is in general larger for more peripheral collisions and scales approximately with the number of participants like $N_{\rm part}^{-1/2}$, in the same way as ε_3 [13]. The variation of $-v_1$ for peripheral collisions is milder than that $\varepsilon_1^{\rm rms}$. This can be attributed to the early freeze-out in peripheral collisions, which has an effect analogous to viscosity and breaks ε_1 scaling.

With bumpy initial conditions, there is no simple direct correspondence between the initial geometry and the final momentum distribution [4]. Figure 5 displays the correlation between the angle of directed flow, Ψ_1, and the angle of the initial dipole asymmetry, Φ_1. The correlation is quite clear, which confirms that the dipole asymmetry is a valid mechanism for generating v_1. However, there is a large dispersion: Some events develop directed flow in a direction very different from the initial dipole asymmetry. A similar dispersion has also been observed for elliptic flow between Ψ_2 and Φ_2 [4] and for triangular flow between Ψ_3 and Φ_3 [36]. The dispersion of $\Psi_1 - \Phi_1$ is qualitatively similar, but much larger. Note that in our calculation, Ψ_1 is determined very accurately for each event, and this dispersion cannot be attributed to a finite event-plane resolution [28].

This large dispersion shows that, although the initial geometry specifies directed flow and Ψ_1 completely, the information on directed flow is not uniquely contained in initial dipole asymmetry. In the language of cumulants [11], the dipole asymmetry represents only the first term in an expansion, and higher-order terms contribute. We have also checked that the distribution of Φ_1 is flat: The direction of the dipole asymmetry is uncorrelated with the reaction plane (which is the x axis in NeXSPheRIO), as expected [11].

Figure 6 displays the values of v_1, averaged over $0 < p_t < 1$ GeV/c, and the initial dipole asymmetry ε_1 for the 120 hydro events used in our analysis. This figure shows that there is no one-to-one correspondence between v_1 and ε_1, though events with a large dipole asymmetry give on average a larger v_1.

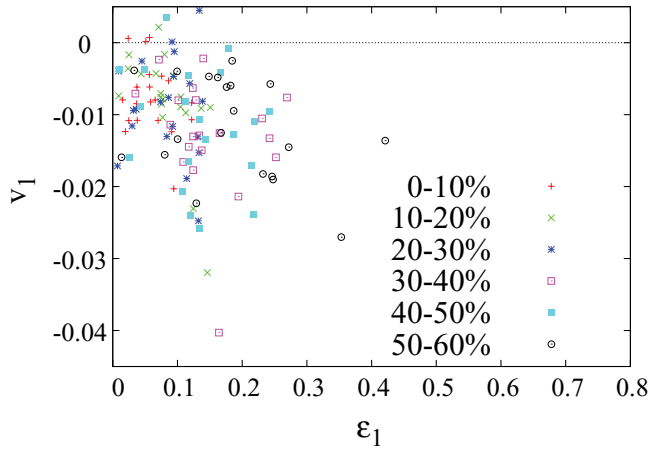

FIG. 6. (Color online) Scatter plot of average v_1 in $0 < p_t < 1$ GeV/c, $|\eta| < 1$ and initial dipole asymmetry ε_1. Results for v_1 are corrected for net transverse momentum.

V. CONCLUSIONS

We have computed the directed flow, v_1, created by initial state fluctuations near midrapidity using event-by-event ideal hydrodynamics for Au-Au collisions at RHIC. This v_1 is an even function of (pseudo)rapidity and has a specific p_t dependence: It is negative below 1 GeV/c and positive above. Its minimum value lies between -0.02 and -0.01 in the centrality range 0%–40%. This is in contrast to the p_t dependence of the usual, rapidity-odd directed flow, which is typically negative for all p_t, both at SPS (see the $v_1\{3\}$ results in Ref. [14]) and at RHIC [15].

The angle of directed flow Ψ_1 is correlated with the angle of the initial dipole asymmetry Φ_1, but with a large dispersion. This confirms the idea of Teaney and Yan that the dipole asymmetry is the mechanism creating v_1. However, it is only a rough picture. Here v_1 is not proportional to ε_1 on an event-by-event basis. More work is needed to understand how fluctuations in the initial geometry are related to final momentum spectra.

Our ideal hydrodynamics results are in remarkable agreement with preliminary experimental results [17,18] inferred from STAR dihadron correlation data in midcentral Au-Au collisions. This quantitative agreement suggests that v_1 is less sensitive to viscosity than v_2 and v_3. Detailed study of v_1 in viscous hydrodynamics is left to future work. Our results establish directed flow at midrapidity as a clear probe of hydrodynamic behavior. Experimental uncertainties on this v_1 are still large, but they can be significantly reduced by carrying out dedicated analyses at RHIC and LHC.

ACKNOWLEDGMENTS

This work is funded by "Agence Nationale de la Recherche" under grant ANR-08-BLAN-0093-01, by Cofecub under project Uc Ph 113/08;2007.1.875.43.9, by FAPESP under projects 09/50180-0, 09/16860-3 and 10/51479-6, and by CNPq under projects 305653/2007-5 and 301141/2010-0.

APPENDIX: INITIAL CONDITIONS FOR EVENT-BY-EVENT HYDRODYNAMICS

In event-by-event hydrodynamics, initial conditions are taken from a microscopic model, which provides an energy-momentum tensor $T^{\mu\nu}$. Since local thermal equilibrium is usually not achieved in the microscopic model, $T^{\mu\nu}$ is not the energy-momentum tensor of an ideal fluid. By switching from the microscopic model to hydrodynamics, one must modify $T^{\mu\nu}$—essentially approximating a yet-unknown thermalization or isotropisation mechanism. In doing so, one must choose quantities to keep continuous during this transformation, while the rest of the energy-momentum tensor necessarily changes discontinuously.

A common procedure is to transform $T^{\mu\nu}$ into the local rest frame [6] where the momentum density T^{0i} vanishes. The fluid velocity is then defined as the velocity of the transformation, and the energy density is defined as $\epsilon \equiv T^{00}$ in the local rest frame. Mathematically, this boils down to a diagonalization of $T^{\mu}_{\ \nu}$ [2]: u^μ is the normalized timelike eigenvector, and ϵ is the corresponding eigenvalue:

$$T^{\mu}_{\ \nu} u^\nu = \epsilon u^\mu. \tag{A1}$$

The pressure P is then defined from ϵ using the equation of state of the fluid, and the energy-momentum tensor of the fluid is defined as usual as $T^{\mu\nu}_{\text{fluid}} = (\epsilon + P)u^\mu u^\nu - P g^{\mu\nu}$. Thus the local rest frame, defined by the fluid velocity u^μ, and the energy density in this frame are chosen to be continuous through the thermalization transformation.

By transforming back to a common laboratory frame, however, it becomes apparent that the energy and momentum density are changed in this process, in an uncontrolled way. For simplicity, consider the case where the transition between the microscopic model and hydrodynamics is done at an initial time t_0 in the laboratory frame. The total energy and momentum of the fluid are the integrals of T^{00} and T^{0i} over the entire space. The above procedure changes T^{00} and T^{0i} and hence violates conservation of energy and momentum, even though the corresponding quantities in the local rest frame $T^{0\mu}_{\text{rest}} \equiv u_\nu T^{\mu\nu}$ are continuous.

Alternatively, rather than demanding continuity of u^μ and ϵ, one can instead choose a procedure that respects conservation of energy and momentum, which we describe here.

It should be noted that the above procedure is not always used [3], and in hydrodynamic calculations without a model for the initial microscopic dynamics (e.g., when only the transverse profile is postulated from a model, while the initial fluid velocity is set by hand) the issue does not arise [4,5].

In general, the transition from the microscopic model to hydrodynamics is done across a spacelike "freeze-in" hypersurface Σ. The total energy and momentum across Σ is

$$P^\mu = \int_\Sigma T^{\mu\nu} d\sigma_\nu, \tag{A2}$$

where $d\sigma_\nu$ is the elementary timelike vector normal to Σ.

Global conservation of energy and momentum demands continuity of P^μ across the freeze-in surface. This can be ensured by demanding *local* energy and momentum conservation ($\partial_\nu T^{\mu\nu} = 0$), which requires continuity of the energy and

momentum flux across the surface. Thus, to generate initial conditions for ideal hydrodynamics in a way that respects energy-momentum conservation laws one must demand local continuity of $T^{\mu\nu}d\sigma_\nu$. For example, in the case of a constant time surface, $d\sigma_\nu \propto (1, 0, 0, 0)$, this amounts to continuity of the energy and momentum density $T^{0\mu}$ [3].

In general, this gives four continuity equations relating the hydrodynamic variables (ϵ, u^μ, P) to the energy-momentum tensor $T^{\mu\nu}$ from the microscopic model:

$$T^{\mu\nu}d\sigma_\nu = (\epsilon + P)u^\mu u^\nu d\sigma_\nu - Pg^{\mu\nu}d\sigma_\nu. \qquad \text{(A3)}$$

Further specifying an equation state $P(\epsilon)$ uniquely determines the hydrodynamic initial conditions, without any additional freedom.

Note that this method agrees with the former method only at points along the freeze-in surface where $d\sigma^\mu \propto u^\mu$, with u^μ defined by Eq. (A1). Everywhere else along the surface, demanding conservation of energy and momentum results in values for ϵ and u^μ in the hydrodynamic phase that are different from those acquired from the microscopic model by Eq. (A1).

[1] M. Luzum, Phys. Lett. B **696**, 499 (2011).
[2] Y. Hama, T. Kodama, and O. Socolowski Jr., Braz. J. Phys. **35**, 24 (2005).
[3] H. Petersen, J. Steinheimer, G. Burau, M. Bleicher, and H. Stocker, Phys. Rev. C **78**, 044901 (2008).
[4] H. Holopainen, H. Niemi, and K. J. Eskola, Phys. Rev. C **83**, 034901 (2011).
[5] B. Schenke, S. Jeon, and C. Gale, Phys. Rev. Lett. **106**, 042301 (2011).
[6] K. Werner, I. Karpenko, T. Pierog, M. Bleicher, and K. Mikhailov, Phys. Rev. C **82**, 044904 (2010).
[7] S. Voloshin and Y. Zhang, Z. Phys. C **70**, 665 (1996).
[8] K. H. Ackermann *et al.* (STAR Collaboration), Phys. Rev. Lett. **86**, 402 (2001).
[9] J. Adams *et al.* (STAR Collaboration), Phys. Rev. Lett. **92**, 062301 (2004).
[10] B. Alver and G. Roland, Phys. Rev. C **81**, 054905 (2010); **82**, 039903(E) (2010).
[11] D. Teaney and L. Yan, arXiv:1010.1876 [nucl-th].
[12] G. Y. Qin, H. Petersen, S. A. Bass, and B. Muller, Phys. Rev. C **82**, 064903 (2010).
[13] B. H. Alver, C. Gombeaud, M. Luzum, and J.-Y. Ollitrault, Phys. Rev. C **82**, 034913 (2010).
[14] C. Alt *et al.* (NA49 Collaboration), Phys. Rev. C **68**, 034903 (2003).
[15] J. Adams *et al.* (STAR Collaboration), Phys. Rev. C **73**, 034903 (2006).
[16] B. I. Abelev *et al.* (STAR Collaboration), Phys. Rev. Lett. **101**, 252301 (2008).
[17] M. Luzum and J. Y. Ollitrault, Phys. Rev. Lett. **106**, 102301 (2011).
[18] H. Agakishiev *et al.* (STAR Collaboration), arXiv:1010.0690 [nucl-ex].
[19] A. L. V. R. dos Reis *et al.* (in preparation).
[20] H. J. Drescher, M. Hladik, S. Ostapchenko, T. Pierog, and K. Werner, Phys. Rep. **350**, 93 (2001).
[21] W. L. Qian, R. Andrade, F. Grassi, O. Socolowski Jr., T. Kodama, and Y. Hama, Int. J. Mod. Phys. E **16**, 1877 (2007).
[22] R. P. G. Andrade, F. Grassi, Y. Hama, T. Kodama, and W. L. Qian, Phys. Rev. Lett. **101**, 112301 (2008).
[23] J. Takahashi *et al.*, Phys. Rev. Lett. **103**, 242301 (2009).
[24] M. Luzum and P. Romatschke, Phys. Rev. C **78**, 034915 (2008); **79**, 039903(E) (2009).
[25] C. Shen, U. Heinz, P. Huovinen, and H. Song, Phys. Rev. C **82**, 054904 (2010).
[26] N. Borghini, P. M. Dinh, and J. Y. Ollitrault, Phys. Rev. C **62**, 034902 (2000).
[27] K. H. Ackermann *et al.* (STAR Collaboration), Nucl. Phys. A **661**, 681 (1999).
[28] A. M. Poskanzer and S. A. Voloshin, Phys. Rev. C **58**, 1671 (1998).
[29] S. S. Adler *et al.* (PHENIX Collaboration), Phys. Rev. C **69**, 034909 (2004).
[30] J. Y. Ollitrault, Nucl. Phys. A **638**, 195 (1998).
[31] N. Borghini and J. Y. Ollitrault, Phys. Lett. B **642**, 227 (2006).
[32] C. Adler *et al.*, (STAR Collaboration), Phys. Rev. C **66**, 034904 (2002).
[33] J. -Y. Ollitrault, A. M. Poskanzer, and S. A. Voloshin, Phys. Rev. C **80**, 014904 (2009).
[34] B. Alver *et al.* (PHOBOS Collaboration), Phys. Rev. Lett. **98**, 242302 (2007).
[35] M. Miller and R. Snellings, arXiv:0312008 [nucl-ex].
[36] H. Petersen, G. Y. Qin, S. A. Bass, and B. Muller, Phys. Rev. C **82**, 041901 (2010).